第 40 卷 第 9 期
2019 年 9 月

焊 接 学 报
TRANSACTIONS OF THE CHINA WELDING INSTITUTION

Vol. 40(9):087 − 092
September 2019

TA2-1060-TA2 复合板爆炸焊接试验及性能测试

房中行[1]， 史长根[1]， 冯 柯[1]， 葛雨珩[2]， 尤 峻[1]
(1. 中国人民解放军陆军工程大学, 南京 210007; 2. 中国空气动力研究与发展中心, 绵阳 621000)

摘 要: 为了解决钛-铝在爆炸焊接过程中可焊性低并容易产生脆性金属间化合物等技术难题, 选用低爆速粉状乳化炸药为试验用药, 下限装药厚度和上限基复板间距为工艺参数, 成功获得了 100% 复合的"1 + 14 + 1"TA2 - 1060 - TA2 双面金属复合板. OM, SEM, EDS 测试结果表明, 复合板界面呈良好小波状结合; 基复板流在波峰阻挡以及复板挤压作用下形成漩涡结构, 其内部存在包覆熔融金属的铸锭组织; 结合界面附件发生不同程度的元素扩散. 力学测试结果表明, 复合板的弯曲强度为 288 MPa、抗拉强度为 165.5 MPa、界面处显微硬度峰值为 227 HV, 满足工业生产要求.

关键词: 爆炸焊接; 结合强度; 小波状结合
中图分类号: TG 456.6 **文献标识码:** A **doi:** 10.12073/j.hjxb.2019400241

0 序 言

单一金属或合金难以满足众多领域对材料性能的综合要求, 国内外学者越来越重视对双层或多层异种金属复合材料的研究. 钛及其合金具有密度小、高耐蚀、比强度大、综合力学性能优良等特性. 铝合金具有密度小、导热和导电性好等特点, 是主要的轻量化结构材料[1-4]. 采用爆炸焊接技术制造的钛-铝-钛双面金属复合材料, 具有轻质高强度、高耐蚀以及成本低等综合优势, 在国防军工和航空航天等领域具有广泛应用前景[5]. 但钛、铝异种金属焊接难度较大, 主要体现在以下几个方面[6-7].

(1) 钛、铝在焊接过程中容易形成多种钛/铝金属间化合物、碳化物和氮化物. 这些化合物的形成会降低焊接接头质量, 增大材料的脆性.

(2) 在焊接过程中氢气在液钛铝和固态钛中可大量溶解, 当焊后温度下降接头凝固时易产生大量气孔, 造成材料塑性和韧性降低.

(3) 钛的导热系数和线胀系数仅为铝的 1/16 和 1/3, 焊接后接头处易产生残余应力形成裂纹.

基于钛、铝在焊接过程中存在的上述问题, 文中提出采用爆炸焊接技术制备钛/铝/钛复合板. 通过金相显微镜 (OM)、扫描电子显微镜 (SEM) 和能谱仪 (EDS), 对钛/铝/钛复合板结合界面形貌和微观结构进行分析, 并进行显微硬度、拉伸和弯曲试验来测试其力学性能.

1 试验方法

采用钛 TA2 作为覆板、铝 1060 作为基板, 进行单面和双面爆炸复合试验, 分别制得 TA2-1060 和 TA2-1060-TA2 金属复合板, 如图 1 所示.

根据装药厚度下限法则和间距上限法则[8-9], 覆板 TA2 厚度为 1 mm, 装药厚度取下限 (单面为 20 mm, 双面为 18 mm), 两板间距取上限为 4 mm. 试验选用低爆速粉状乳化炸药, 添加 30% 石英砂, 控制其爆速约为 2 000 m/s. 为了消除边界效应的影响, 采用短边中心起爆方式, 覆板尺寸和装药面积在起爆端增加 30 mm、在两侧和尾端分别增加 20 和 40 mm, 基板尺寸为 550 mm × 250 mm × 14 mm, 进而确定覆板尺寸为 620 mm × 290 mm × 1 mm.

为观察复合板结合界面形貌和进行力学性能测试, 并尽可能节约复合板材料, 避免对界面组织产生影响, 设计了如图 2 所示的线切割方案. 其中图 2a 为单面方案, 图 2b 为双面方案. 表 1 所示为切割试样的具体测试内容. 图 2 与表 1 所示试样编号相对应.

收稿日期: 2018 − 03 − 07
基金项目: 国家自然科学基金资助项目 (51541112)

(a) 双层复合板 (b) 三层复合板

图 1 钛-铝和钛-铝-钛复合板

Fig. 1 TA2-1060 and TA2-1060-TA2 cladding plates

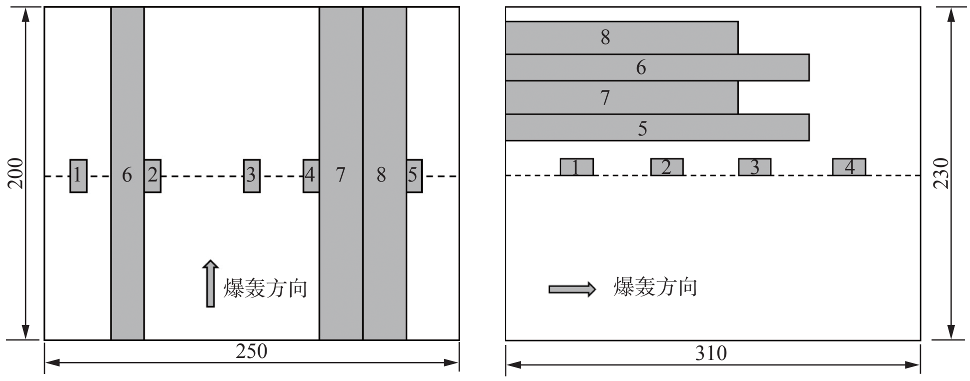

(a) 单面 (b) 双面

图 2 试样切割方案 (mm)

Fig. 2 Line cutting scheme of the samples

表 1 试样测试内容

Table 1 Content of the sample tests

测试内容	OM, SEM, EDS	拉伸测试	弯曲测试
单面	1 ~ 5	6	7, 8
双面	1 ~ 4	5, 6	7, 8

2 界面形貌和微观结构分析

2.1 界面波形特征分析

图 3 为金相显微镜拍摄的结合界面形貌. 图 3a ~ 图 3e 试样为第一次爆炸后界面, 其中上层为铝 1060, 下层为钛 TA2; 图 3f ~ 图 3i 为第二次爆炸后的界面, 其中上层为钛 TA2, 下层为铝 1060. 金相照片显示 TA2 - 1060 结合界面呈波状结合. 以图 3a ~ 图 3d 界面为例, 波形大小逐渐增大, 图 3a 和图 3b 显示波形呈微波状, 图 3c 开始波形显著变大, 而后波形逐渐稳定为小波状. 波状结合可以增大界面的接触面积, 形成锯齿状咬合, 而合理的波形大小通常表明界面较高的结合强度. 微小波状结合能够节约更多装药量, 而结合强度却大幅提高[10-11].

由于降低了装药量, 双面复合板结合界面的波形比单面复合板更小, 因此结合质量更高. 靠近钛侧界面处出现细碎晶粒组织, 晶粒大小约为 10 μm, 晶粒形态符合铸锭组织结晶特征, 远离界面处晶粒形态与原始组织相同

2.2 漩涡形成机理分析

图 4 为单面和双面复合板漩涡分布及其典型的微观结构. 可以看出, 漩涡结构并非偶然或随机分布, 而是有规律地出现在覆板隆起部分, 即漩涡结构周期性的形成于界面波峰处.

漩涡结构是波状结合界面的一个典型特征. 基板和覆板发生倾斜碰撞时, 碰撞点处覆板向基板侵入使基板上形成凹陷, 而在碰撞点前方, 基板在金属射流的剪切作用下凸起形成波峰. 在爆炸载荷产生的巨大弯矩以及高温高压作用下, 覆板和基板表面呈现流体状态, 覆板流和基板流分别以逆时针和顺时针方向旋转. 覆板流在波峰的阻挡以及覆板的挤压作用下, 在波峰后沿形成覆板漩涡, 而基板流在越过波峰后在波峰前沿形成基板漩涡. 漩涡结构

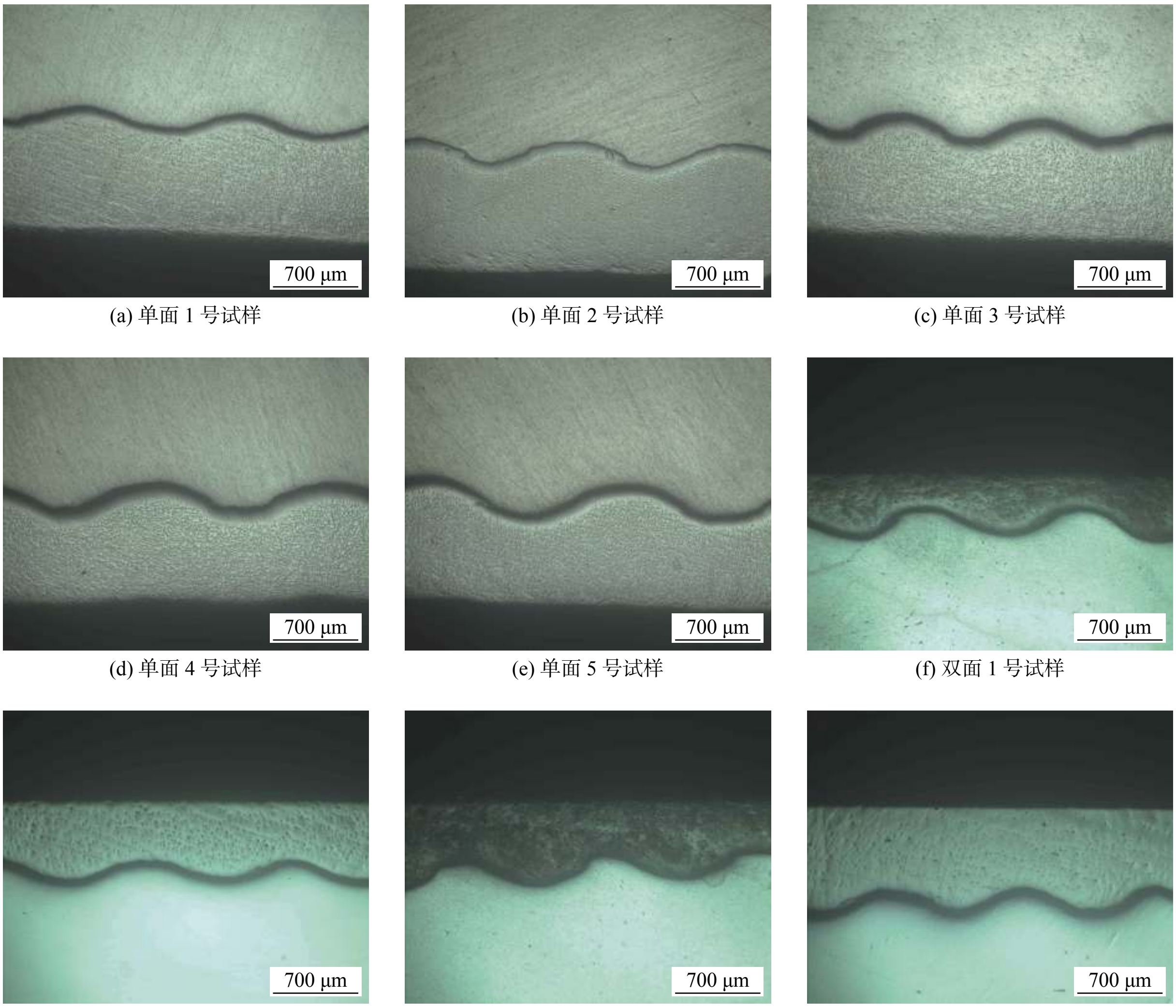

(a) 单面 1 号试样　(b) 单面 2 号试样　(c) 单面 3 号试样

(d) 单面 4 号试样　(e) 单面 5 号试样　(f) 双面 1 号试样

(g) 双面 2 号试样　(h) 双面 3 号试样　(i) 双面 4 号试样

图 3　TA2 - 1060 - TA2 结合界面金相照片

Fig. 3　Metallographic photos of TA2 - 1060 - TA2 bonding interface

内为铸锭组织，如图 4c 所示，随着漩涡结构的形成，界面处可能产生的熔融金属被包裹在其中，使结合界面无法形成连续熔化层，一定程度上有利于提高复合板的结合强度.

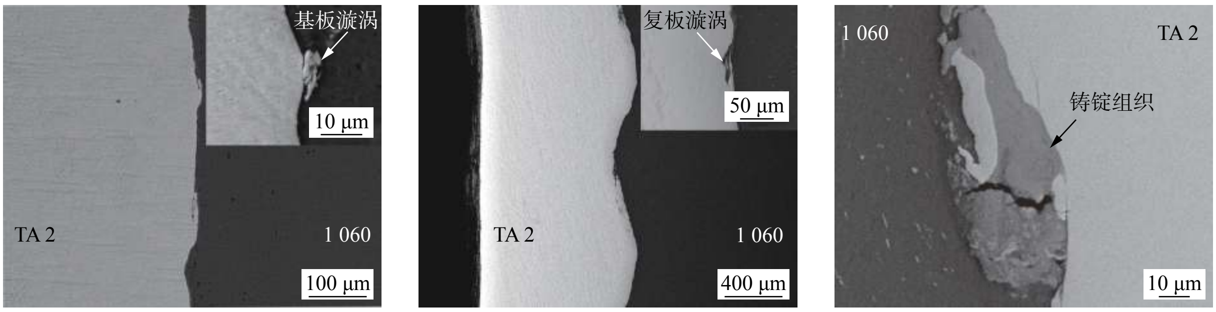

(a) 单面复合板漩涡　(b) 双面复合板漩涡　(c) 漩涡内铸锭组织

图 4　结合界面漩涡结构

Fig. 4　Vortex structure at the bonding interface

2.3　界面扩散现象

在结合界面附近进行元素线扫描测试，结果如图 5 所示. 可以看出，结合界面附近钛和铝元素质量分数发生突变，扩散曲线呈现“X”形交叉，说明在界面附近基板和覆板金属元素发生了扩散，金属原子互相交错. 其中单面复合板结合界面的元素扩散层

厚度约为 3.2 μm, 双面复合板结合界面元素扩散层厚度约为 2.4 μm, 其元素扩散层厚度比单面复合板薄.

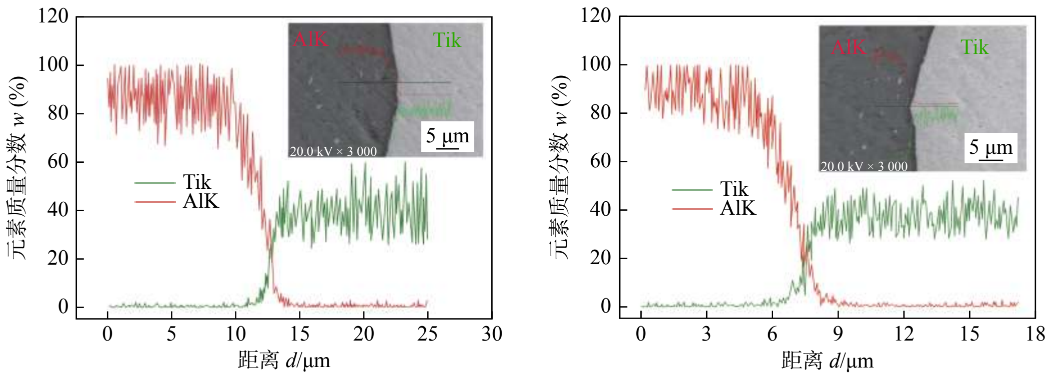

(a) 单面复合板界面元素扩散 (b) 双面复合板元素扩散

图 5 结合界面元素扩散

Fig. 5 Elemental diffusion at the bonding interfaces

一方面, 由于装药厚度的降低, 双面复合时基板和覆板碰撞能量以及界面元素扩散驱动力减小; 另一方面, 由于 18 mm 装药量更接近于装药厚度下限, 减小了界面熔化, 界面金属原子扩散增强了基复板间的吸引力, 能够使复合板结合强度显著提高.

2.4 绝热剪切现象

复合板结合界面处可以观察到一些向基板和覆板侧延伸的黑色线条, 如图 6 所示. 这些线条以界面为包络线、与界面约成 45 °, 被称为“绝热剪切线”. 绝热剪切线从结合界面向基板和覆板金属基体延伸, 其本质是塑性变形由界面向材料基体的延伸[12]. 绝热剪切线的形成与材料的冲击韧性以及爆炸载荷有关, 由于钛和铝的冲击韧性均较小, 在爆炸焊接中结合界面附近容易产生绝热剪切线.

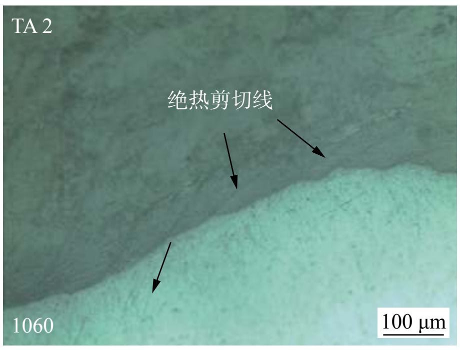

图 6 绝热剪切线

Fig. 6 Adiabatic shear line

图 6 中绝热剪切线的长度约为 150 ~ 200 μm. 绝热剪切线实际上是一种裂纹源, 它是基板和覆板表面产生宏观裂纹的微观反应, 其长度大于 500 μm 时容易发展成微裂纹, 故绝热剪切线的存在将对复合板结合质量产生不利影响. 为减少爆炸焊接中产生大量绝热剪切线, 可在焊接前通过热处理方法降低材料强度提高塑性和韧性. 此外, 选用低爆速炸药、采用下限装药量和上限间距的工艺参数, 也能有效减少不利影响.

3 力学性能测试与分析

3.1 弯曲试验

为测试复合板承受弯曲应力的能力, 对图 2 中的弯曲试样 (尺寸为 200 mm × 20 mm × 15 mm) 加载弯曲载荷, 分别进行了内弯 (TA2 在内侧) 和外弯 (TA2 在外侧) 试验, 并观察结合界面是否发生分层和开裂. 结果如图 7 所示, 内弯试样结合界面和材料基体均完好, 而外弯试样 TA2 一侧发生了开裂, 但结合界面并未分层, 这说明复合板的结合强度基本符合要求. TA2 侧的开裂可能是由于其在爆炸载荷的直接作用下发生剧烈的塑性变形, 造成爆炸硬化, 进而导致塑性和韧性降低.

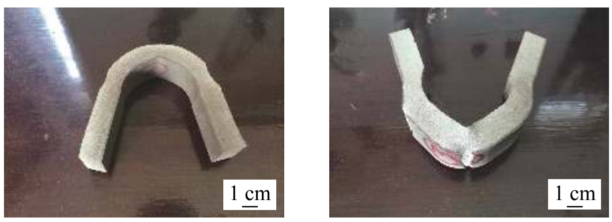

(a) 内弯试样 (b) 外弯试样

图 7 弯曲试样

Fig. 7 The samples for bending test

图 8 为复合板弯曲载荷曲线, 内弯和外弯试样

所能承受载荷 F 均约为 48 kN. 由于外弯试样 TA2 侧开裂, 在 530 s 后即发生卸载. 根据试验结果计算得到复合板弯曲强度为 288 MPa.

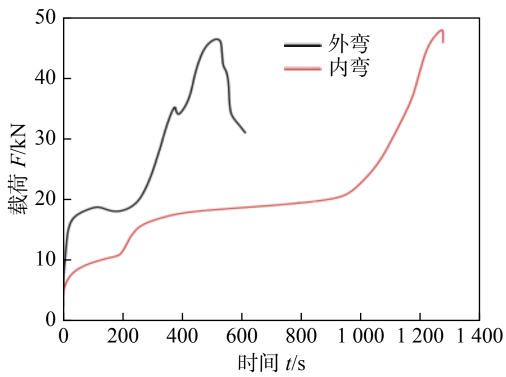

图 8　弯曲载荷曲线

Fig. 8　Bending load curves

3.2　拉伸试验

采用全厚度拉伸方法 (试样厚度小于 50 mm) 对单面试样和双面试样分别进行拉伸测试, 拉伸结果如图 9 所示. 单面和双面复合板拉伸载荷曲线均符合材料拉伸四个阶段特征, 如图 10 所示. 图 10 中 c(c') 点拉力达到最大值, 即达到材料的抗拉强度, 到 d(d') 点处试样被拉断. 由试验数据可计算得到双面复合板抗拉强度为 165.5 MPa, 符合国家标准要求.

图 9　拉伸试样

Fig. 9　The samples for tensile test

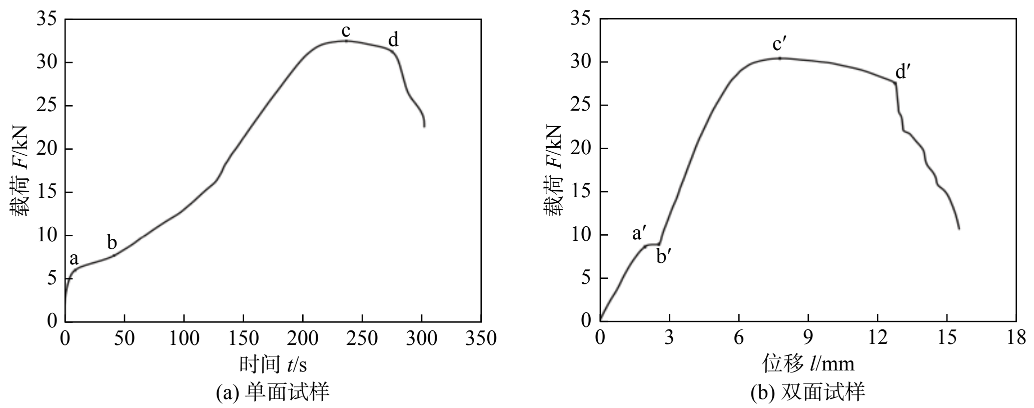

图 10　拉伸载荷曲线

Fig. 10　Tensile load curves

3.3　显微硬度试验

显微硬度用来衡量材料抵抗外力压入引起塑性变形的能力. 采用压入法对试样界面附近显微硬度进行测试, 测试点间距为 0.15 mm, 测试结果如图 11 所示. 在离界面约 300 μm 处显微硬度值接近基板和覆板基体材料硬度, 离界面越近硬度越大, 在结合界面处显微硬度达到最大值 227 HV. 结合界面附近晶粒组织较为细小, 爆炸焊接极大的过冷度对界面产生了细晶强化作用, 因此结合界面处的显微硬度值最大. 远离界面的金属显微硬度稍大于基体材料硬度, 这是由于在巨大的爆炸载荷作用下, 基板和覆板整体均发生一定程度的塑性变形, 导致加工硬化.

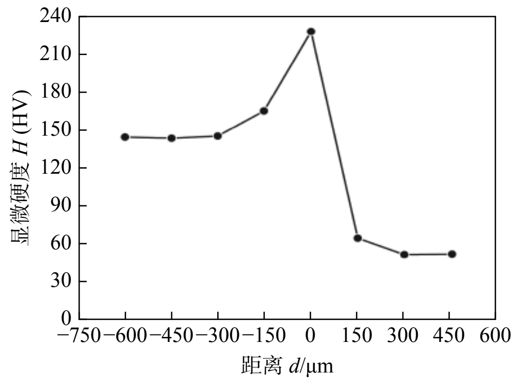

图 11　结合界面附近显微硬度分布曲线

Fig. 11　Microhardness distribution curve near the bonding interface

4　结　论

(1) 通过爆炸焊接成功制造了钛-铝单面和双面金属复合板,其结合界面均呈现小波状形貌.

(2) 钛-铝爆炸焊接复合板结合界面附近出现绝热剪切线,界面波峰处有规律地形成漩涡结构,其内为铸锭组织.

(3) 钛-铝爆炸焊接复合板结合界面附近发生元素扩散,单面和双面复合板元素扩散层厚度分别约为 3.2 和 2.4 μm.

(4) 钛-铝爆炸焊接复合板的弯曲强度为 288 MPa,抗拉强度为 165.5 MPa,结合界面附近显微硬度最大值为 227 HV,符合工业生产要求.

参考文献:

[1] 韩小敏, 王少刚, 黄　燕, 等. TA10-Q345R 爆炸复合板的界面微观结构及力学性能 [J]. 压力容器, 2015, 32(6): 24 − 29.
Han Xiaomin, Wang Shaogang, Huang Yan, *et al*. Interfacial microstructure and mechanical properties of TA10-Q345R composite plate with explosive welding[J]. Pressure Vessel Technology, 2015, 32(6): 24 − 29.

[2] Mali V I, Bataev A A, Maliutina I N, *et al*. Microstructure and mechanical properties of Ti/Ta/Cu/Ni alloy laminate composite materials produced by explosive welding[J]. International Journal of Advanced Manufacturing Technology, 2017, 93: 4285 − 4294.

[3] 陈　沛, 段卫东, 曾国伟, 等. 钛/钢爆炸焊接界面波形及缺陷组织的形成机理 [J]. 爆破, 2019, 36(1): 126 − 132.
Chen Pei, Duan Weidong, Zeng Guowei, *et al*. Formation mechanism of interface waveform and defect microstructure in Ti / steel explosive welding[J]. Blasting, 2019, 36(1): 126 − 132.

[4] Zhang M, Zhang T, Cai J Q, *et al*. Effect of heat treatment on microstructure and properties of explosive welding clad plate of TA1/Q345[J]. China Welding, 2018, 27(1): 26 − 31.

[5] Bataev I A, Bataev A A, Mali V I, *et al*. Structural and mechanical properties of metallic-intermetallic laminate composites produced by explosive welding and annealing[J]. Materials & Design, 2012, 35: 225 − 234.

[6] Fronczek D M, Wojewoda-Budka J, Chulist R, *et al*. Structural properties of Ti/Al clads manufactured by explosive welding and annealing[J]. Materials & Design, 2016, 91: 80 − 89.

[7] 范敏郁, 郭训忠, 崔圣强, 等. 钛/铝/钛三层板的一次爆炸复合 [J]. 稀有金属材料与工程, 2017, 46(3): 770 − 776.
Fan Minyu, Guo Xunzhong, Cui Shengqiang, *et al*. One-step explosive bonding preparation of titanium/aluminum/titanium laminates with three layers[J]. Rare Metal Materials and Engineering, 2017, 46(3): 770 − 776.

[8] 史长根, 杨　旋, 侯鸿宝, 等. 爆炸焊接两板间距上限法则分析与试验 [J]. 焊接学报, 2018, 39(1): 1 − 4.
Shi Changgen, Yang Xuan, Hou Hongbao, *et al*. Analysis and experiment on upper limit law of two plates stands in explosive welding[J]. Transactions of the China Welding Institution, 2018, 39(1): 1 − 4.

[9] Shi C G, Wang Y, Li S J, *et al*. Application and experiment on the least-action principle of explosive welding of stainless steel / steel[J]. Journal of Iron and Steel Research (International), 2014, 21(6): 625 − 629.

[10] Xia H B, Wang S G, Ben H F. Microstructure and mechanical properties of Ti/Al explosive cladding[J]. Materials & Design, 2014, 56: 1014 − 1019.

[11] Zhang L J, Pei Q, Zhang J X, *et al*. Study on the microstructure and mechanical properties of explosive welded 2205 / X65 bimetallic sheet[J]. Materials & Design, 2014, 64: 462 − 476.

[12] 张婷婷, 王文先, 魏　屹, 等. 钛/铝/镁爆炸焊复合板波形界面及力学性能 [J]. 焊接学报, 2017, 38(8): 33 − 36.
Zhang Tingting, Wang Wenxian, Wei Yi, *et al*. Wavy interface and mechanical properties of explosive welded Ti/Al/Mg cladded plate[J]. Transactions of the China Welding Institution, 2017, 38(8): 33 − 36.

第一作者简介: 房中行, 男, 1995 年出生, 硕士研究生. 主要从事材料加工成形和金属复合材料方面的研究工作. 发表论文 2 篇. Email: fangzhonghang@foxmail.com
通信作者简介: 史长根, 男, 副教授. Email: shichanggen71@sina.com

improve the horizontal welding quality.

Key words: local dry welding; horizontal welding; metal transfer; GMAW

Explosive welding experiment and property test of TA2-1060-TA2 cladding plate FANG Zhonghang[1], SHI Changgen[1], FENG Ke[1], GE Yuheng[2], YOU Jun[1] (1. Army Engineering University of PLA, College of Field Engineering, Nanjing 210007, China; 2. High Speed Institute of China Aerodynamics Research & Development Center, Mianyang 621000, China). pp 87-92

Abstract: To solve technical problems of low weldability and easy generation of brittle intermetallic compounds during titanium-aluminum explosive welding, the low-detonation-velocity powdery emulsion explosive, lower limit of charge thickness and upper limit of distance between the flyer and base plates were determined, thereby successfully manufacturing "1 + 14 + 1" TA2-1060-TA2 double-sided metal cladding plate with 100 % welding rate. The results of OM, SEM, EDS tests showed that the interfaces of the cladding plate presented the high quality small wavy bonding; under the action of peak blocking and flyer plate extrusion, the flowing of the base and flyer plates generated the vortex structure where the ingot structure wrapping molten metals were observed; different levels of elemental diffusion took place near the bonding interfaces. The mechanical test results showed that the bending strength, tensile strength and microhardness peak value of the cladding plate were 288 MPa, 165.5 MPa and 227 HV, respectively, which met the requirements of industrial production.

Key words: explosive welding; bonding strength; small wave bonding

Effect of energy director on microstructure and mechanical properties of CF/PEEK joints obtained by ultrasonic welding ZHANG Zenghuan[1], SU Xuan[2], LI Hao[1], TAO Wang[2], WANG Yuhua[1] (1. Shanghai Aircraft Manufacturing Co., Ltd., Shanghai 200436, China; 2. State Key Laboratory of Advanced Welding and Joining, Harbin Institute of Technology, Harbin 150001, China). pp 93-98

Abstract: The ultrasonic welding was employed to connect carbon-fiber-reinforced polyetherether-ketone (CF/PEEK) composites. The effects of the shapes of energy directors (ED) on the microstructure and mechanical property of joints were mainly investigated. The results showed that the heat affected zone (HAZ) of the joints was larger when the rectangular or triangular ED were used, which was caused by the high viscoelastic deformation of EDs, rapid heating rate at the interface and high interface temperature. Thermal stress was larger at the interface between carbon fiber and resin in the HAZ, which easily resulted in cracks and other defects. In addition, the flow pattern of ED made void defects easily occurred. Therefore, the joints had poor mechanical property. When flat ED was used, the interface formed a good connection with ultrasonic action time of 0.9 s. The flow pattern of flat ED was better than that of the rectangular and triangular ED, so no void defects occurred in joints whose tensile-shear strength could reach 28 MPa.

Key words: ultrasonic welding; CF/PEEK; energy directors; interface temperature; mechanical property

Characteristic of titanium/steel dissimilar metals joint brazed by bypass-current arc welding MIAO Yugang[1], LIN Zhicheng[1], ZOU Junpan[2], GUO Junliang[2], HAN Duanfeng[2] (1. National Key Laboratory of Science and Technology on Underwater Vehicle, Harbin Engineering University, Harbin 150001, China; 2. College of Shipbuilding Engineering, Harbin Engineering University, Harbin 150001, China). pp 99-103

Abstract: The titanium and steel dissimilar metals were brazed by bypass-current arc welding with S211 copper alloy as filler metal. The macro and microstructure, element distribution, and tensile strength of the brazed joints were analyzed by using optical microscopy, scanning electron microscopy, universal tensile testing machine and other technologies, and the hardness distribution of joint was analyzed by using a micro-hardness tester. A well brazed joint of titanium/steel was obtained, and no obvious welding defects were found. Hardness test found that the hardness in the titanium/copper area was significantly increased, and this was related to the easy formation of Ti-Cu intermetallic compound in the titanium/copper area. The fracture of the titanium/steel brazed joint occured on the copper/titanium side, the fracture mode was ductile-brittle mixed fracture, and the tensile strength reached 291.55 MPa, which was about 88% of the strength of the copper solder.

Key words: Ti/steel dissimilar metal; bypass-current arc brazing; element analysis; tensile strength; hardness

Design modeling and experimental verifications of the laminated busbar for high frequency arc welding inverter HE Yaning, XIONG Gang (Chengdu Xionggu Jiashi Electrical Co., Ltd., Chengdu 611731, China). pp 104-110

Abstract: With the increase of switching frequency, reducing stray inductance becomes one of the key factors in designing high frequency arc welding inverter. In order to meet the demand of DPS-500 of 50 kHz/20 kW, a laminated busbar was designed, which integrated DC link capacitor, soft start circuit, IGBT module and three-phase rectifier module. The numerical calculation of quasi-static electromagnetic field was carried out using ANSYS Q3D. Parasitic parameter matrices were extracted. The multi-port circuit model of the